Application of the Coupled FE-EFG Method to Material Discontinuities in 1D and 2D

N. Sukumar

May 27, 1996

1 One-Dimensional Problems

1.1 Problem Statement

Consider the following one-dimensional Dirichlet boundary-value problem (strong form):

$$
\begin{aligned}
-\frac{d}{dx}\left(E\frac{du}{dx}\right) &= b \quad \text{in } \Omega\,, \\
u(0) &= \bar{u}_1\,, \\
u(L) &= \bar{u}_2\,, \\
\left[\!\left[E\frac{du}{dn} \right]\!\right] &= 0 \quad \text{on } \Gamma \quad \text{(jump condition)}
\end{aligned}
\tag{1}
$$

where $\Omega = \{x \mid x \in (0, L)\}$, $\Omega = \Omega_1 \cup \Omega_2$. The elastic constant E is smooth in Ω_1 and Ω_2, but is discontinuous at the interface Γ between Ω_1 and Ω_2.

We seek trial functions $u^h(x) \in \mathcal{H}^1(\Omega)$ such that (weak/variational form)

$$
\int_\Omega E\frac{du^h}{dx}\frac{dv^h}{dx}\,dx = \int_\Omega b v^h\,dx\,, \quad \forall\ v^h \in \mathcal{H}^h\ (\mathcal{H}^h \subset \mathcal{H}^1_0) \tag{2}
$$

1.2 Bi-Material Bar

Consider a bi-material bar of length L (Figure 1) with material moduli E_1 in Ω_1 and E_2 in Ω_2. The interface Γ is located at $x = x_s$. The domain is discretized by FE- as well as EFG-nodes. Kinematic admissibility is met by choosing FE nodes at $x = 0$ and $x = L$; in addition, an FE node at the interface point ensures displacement continuity and the approximate satisfaction of the natural boundary (jump) condition (in the "weak" sense). All the other nodes have EFG-character! The nodal discretization for $L = 1$ using 17 equi-spaced nodes (18 cells) is shown in Figure 2 ($x_s = 0.25$).

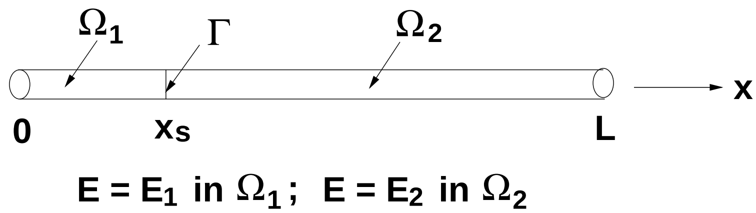

Figure 1: One-dimensional bi-material bar

A linear basis function ($p = \{1, x\}$), quartic polynomial weight function, and a linear ramp are used to construct the shape functions (EFG and interface). Numerical integration is carried out using four-point Gauss quadrature. The support for the weight function is: $d_{mI} = d_{\max} c$, where $c = \alpha c_I$. In the analysis, $d_{\max} = 3.2$ and $\alpha = 1.001$. The parameter c_I is the distance to the 2^{nd} nearest neighbor from node I.

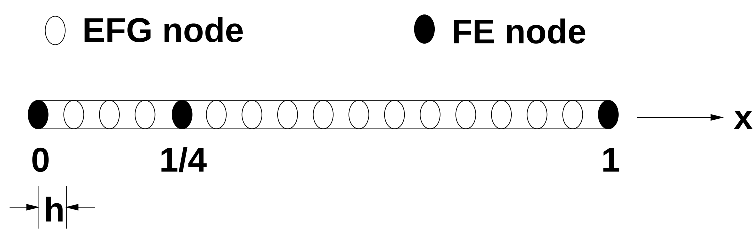

Figure 2: Nodal discretization

1.3 Numerical Solution

1.3.1 Example 1

Consider a bi-material patch test: $\bar{u}_1 = 0$, $\bar{u}_2 = 1$ and $b(x) = 0$. The exact solution in terms of E_1, E_2 and x_s is:

$$u(x) = \begin{cases} \frac{E_2}{(E_2 - E_1)x_s + E_1} x\,, & 0 \leq x \leq x_s \\ \frac{E_1}{(E_2 - E_1)x_s + E_1}(x-1) + 1\,, & x_s \leq x \leq 1 \end{cases} \tag{3}$$

In Figures 3a and 3b, the numerical and exact (displacement and strain) solutions are presented for two cases: (a) $E_1 = 10^4$, $E_2 = 10^3$ and (b) $E_1 = 10^4$, $E_2 = 10^2$. The nodal discretization shown in Figure 2 is used ($x_s = 0.25$).

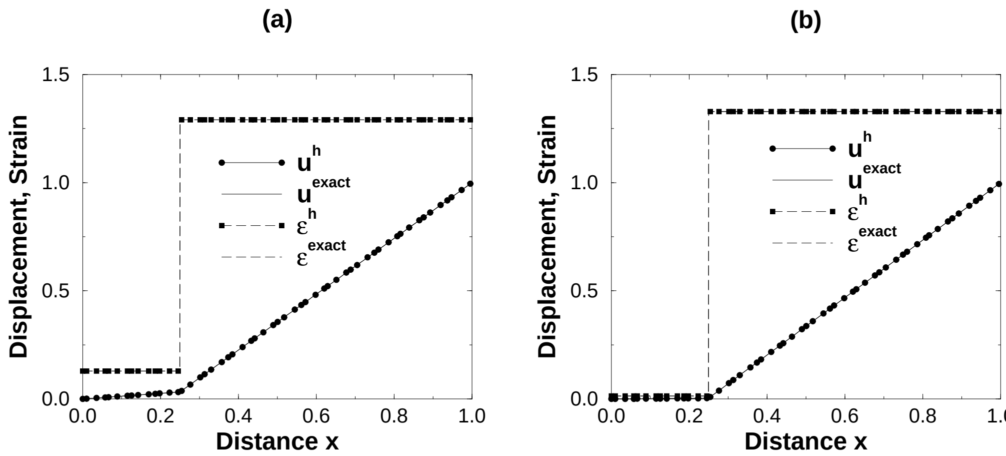

Figure 3: Comparison of numerical and exact solution (Example 1). (a) $E_1 = 10^4$, $E_2 = 10^3$; (b) $E_1 = 10^4$, $E_2 = 10^2$

1.3.2 Example 2

Let $\bar{u}_1 = 0$, $\bar{u}_2 = 0$ and $b(x) = -2$. The exact solution is now a quadratic in x:

$$u(x) = \begin{cases} \frac{x^2-\alpha x}{E_1}, & 0 \le x \le x_s \\ \\ \frac{x^2-1-\alpha(x-1)}{E_2}, & x_s \le x \le 1 \end{cases} \tag{4}$$

where

$$\alpha = \frac{x_s^2(E_2 - E_1) + E_1}{x_s(E_2 - E_1) + E_1}\,. \tag{5}$$

The nodal discretization shown in Figure 2 is used. In Figures 4a and 4b, the numerical and exact (displacement and strain) solutions are illustrated for $E_1 = 10^4$, $E_2 = 10^3$ and $x_s = 0.25$. In Figure 5, the $\mathcal{L}_2$- and $\mathcal{H}^1$-error norms ($E_1 = 10^4$, $E_2 = 10^3$ $x_s = 0.25$) are shown as a function of the nodal spacing on a log-log plot. The error norm results are computed for four different nodal spacings: $h = \bar{h}/16$, $\bar{h}/8$, $\bar{h}/4$ and $\bar{h}$, where $\bar{h} = 0.125$. The $\mathcal{L}_2$- and $\mathcal{H}^1$-error norms are given by:

$$\|e\|_0 = \sqrt{\int_\Omega e^2\,dx}\,,\ \ \|e\|_1 = \sqrt{\int_\Omega (e^2 + e'^2)\,dx}\ , \tag{6}$$

where $e = u - u^h$. It is observed that the convergence rates for the displacement and strains are 2.39 and 0.95, respectively.

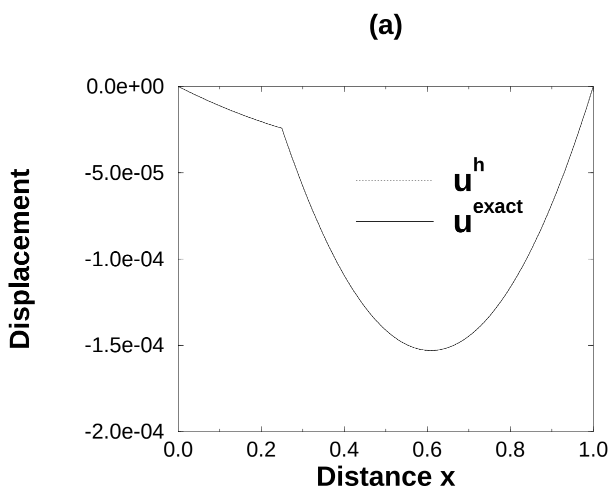

Figure 4: Comparison of numerical and exact solution for $E_1 = 10^4$, $E_2 = 10^3$, $x_s = 0.25$ (Example 2). (a) Displacement; (b) Strain

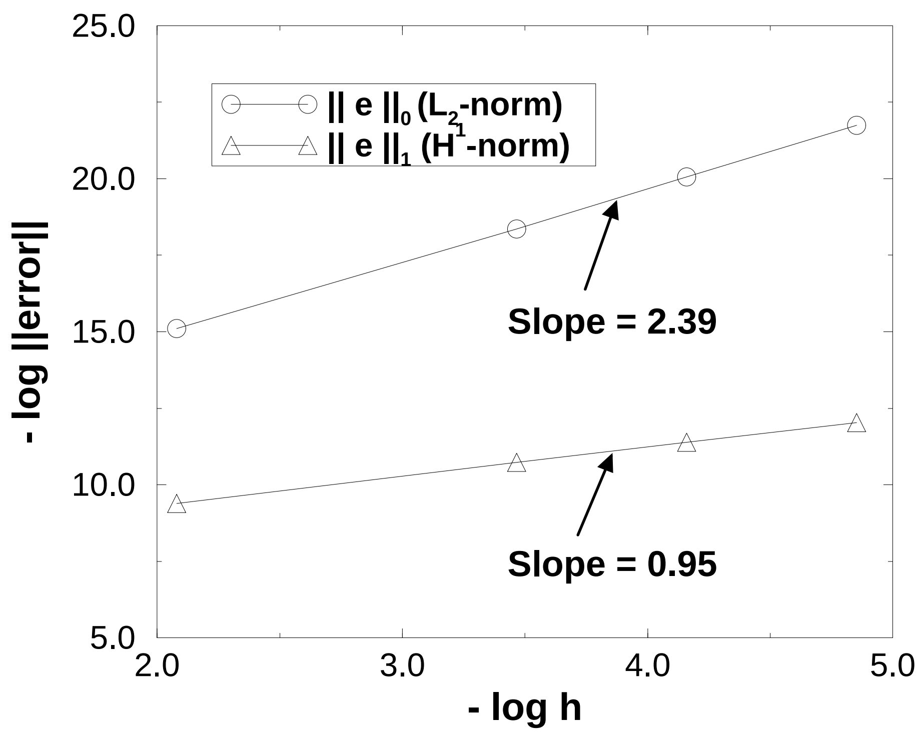

Figure 5: Rate of convergence for $\mathcal{L}_2$ and $\mathcal{H}^1$ error norms

1.3.3 Example 3

The Dirichlet boundary data are chosen as: $\bar{u}_1 = 0$, $\bar{u}_2 = 0$, while the body force $b(x) = -4e^{-2x}$ (Mackinnon and Carey, IJNME, 1987). The analytic solution is:

$$u(x) = \begin{cases} \frac{e^{-2x} - 1 + \alpha x}{E_1}, & 0 \leq x \leq x_s \\ \frac{e^{-2x} - e^{-2} + \alpha(x-1)}{E_2}, & x_s \leq x \leq 1 \end{cases} \tag{7}$$

where

$$\alpha = \frac{e^{-2x_s}(E_2 - E_1) + E_1 e^{-2} - E_2}{x_s(E_1 - E_2) - E_1}. \tag{8}$$

Let the location of the interface $x_s = 0.5$. The domain is discretized by 17 nodes: 3 FE nodes and the rest are EFG nodes. In Figures 6a and 6b, the numerical and exact solutions are compared for $E_1 = 10^4$ and $E_2 = 10^3$. In Figure 7, the $\mathcal{L}_2$- and $\mathcal{H}^1$-error norms are plotted as a function of h ($h = \bar{h}/8$, $\bar{h}/4$, $\bar{h}/2$ and $\bar{h}$, where $\bar{h} = 0.125$) on a log-log plot. The convergence rates for u and ε are 2.51 and 0.96, respectively.

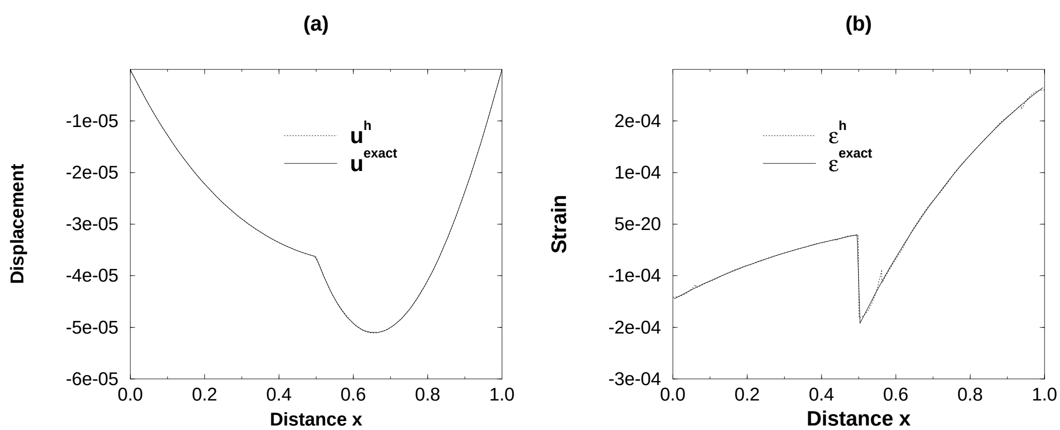

Figure 6: Comparison of numerical and exact solution for $E_1 = 10^4$, $E_2 = 10^3$, $x_s = 0.5$ (Example 3). (a) Displacement; (b) Strain

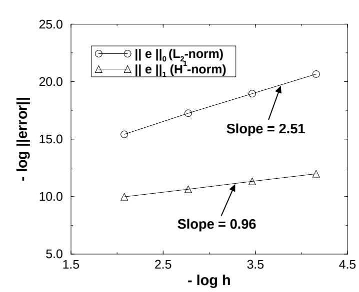

Figure 7: Rate of convergence for $\mathcal{L}_2$ and $\mathcal{H}^1$ error norms

2 Two-Dimensional Problem

2.1 Bi-material Boundary-Value Problem

In Figure 8a, a body ($\mathbf{x} \in \mathcal{R}^2$) composed of two different materials (bi-material) is shown. The material properties are constants in Ω_1 and Ω_2, but there is a discontinuity in the material constants across the interface Γ_1 ($r = r_i$). The Lamè constants in Ω_1 are chosen as: $\lambda_1 = 497.16$, $\mu_1 = 390.63$, while those in Ω_2 are: $\lambda_2 = 656.79$, $\mu_2 = 338.35$. These correspond to $E_1 = 1000$, $\nu_1 = 0.28$, and $E_2 = 900$, $\nu_2 = 0.33$.

2.2 Boundary Conditions and Exact Solution

We impose the linear displacement field: $u_1 = x_1$, $u_2 = x_2$ ($u_r = r$, $u_\theta = 0$ in polar coordinates) on the boundary Γ_2. The Navier's equation in polar coordinates reduces to ($u_r = u_r(r)$, $u_\theta = 0$):

$$\frac{1}{r}\frac{d}{dr}\left[\frac{d}{dr}(ru_r)\right] = 0\,. \tag{9}$$

By considering displacement and traction continuity across the interface, the exact displacement solution can be written as

$$\begin{aligned} u_r &= \begin{cases} \left[\left(1 - \frac{R^2}{r_i^2}\right)\alpha + \frac{R^2}{r_i^2}\right] r\,, & 0 \le r \le r_i \\ \left(r - \frac{R^2}{r}\right)\alpha + \frac{R^2}{r}\,, & r_i \le r \le R \end{cases} \\ u_\theta &= 0 \end{aligned} \tag{10}$$

where

$$\alpha = \frac{(\lambda_1 + \mu_1 + \mu_2)R^2}{(\lambda_2 + \mu_2)r_i^2 + (\lambda_1 + \mu_1)(R^2 - r_i^2) + \mu_2 R^2} \tag{11}$$

The radial (ε_{rr}) and hoop ($\varepsilon_{\theta\theta}$) strains are given by

$$\begin{aligned} \varepsilon_{rr} &= \begin{cases} \left(1 - \frac{R^2}{r_i^2}\right)\alpha + \frac{R^2}{r_i^2}\,, & 0 \le r \le r_i \\ \left(1 + \frac{R^2}{r^2}\right)\alpha - \frac{R^2}{r^2}\,, & r_i \le r \le R \end{cases} \\ \varepsilon_{\theta\theta} &= \begin{cases} \left(1 - \frac{R^2}{r_i^2}\right)\alpha + \frac{R^2}{r_i^2}\,, & 0 \le r \le r_i \\ \left(1 - \frac{R^2}{r^2}\right)\alpha + \frac{R^2}{r^2}\,, & r_i \le r \le R \end{cases} \end{aligned} \tag{12}$$

The radial (σ_{rr}) and hoop ($\sigma_{\theta\theta}$) stresses are:

$$\begin{aligned} \sigma_{rr} &= 2\mu\varepsilon_{rr} + \lambda(\varepsilon_{rr} + \varepsilon_{\theta\theta})\,, \\ \sigma_{\theta\theta} &= 2\mu\varepsilon_{\theta\theta} + \lambda(\varepsilon_{rr} + \varepsilon_{\theta\theta})\,, \end{aligned} \tag{13}$$

where the appropriate Lamè constants are to be used in the evaluation of the stresses. The shear components of the stress and strain tensors are zero.

2.3 Numerical Solution

Due to symmetry, one-quarter of the domain is modeled. The domain is discretized using 257 nodes: 67 FE nodes (on the boundary and along the interface $r = r_i$) and 190 EFG nodes (Figure 8b). Numerical integration is carried out using 4×4 Gauss quadrature; quartic polynomial weight function with $d_{max} = 4.0$ is used. Due to axi-symmetry, results are presented as a function of r along $\theta = 0°$. In Figure 9, the exact and numerical solutions for u_r and u_θ are shown. The comparisons for the radial strain ε_{rr} and hoop strain $\varepsilon_{\theta\theta}$ are presented in Figures 10a and 10b, while those for the radial stress σ_{rr} and hoop stress $\sigma_{\theta\theta}$ are shown in Figures 11a and 11b.

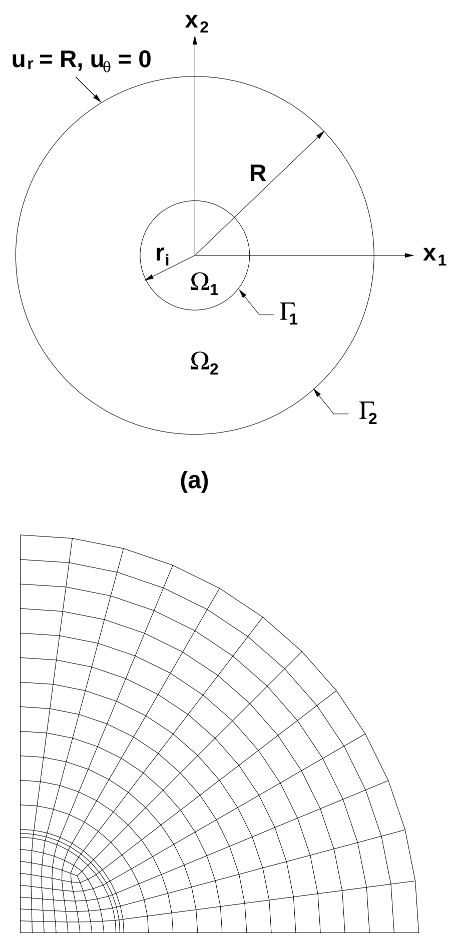

Figure 8: Bimaterial boundary-value problem. (a) Domain and BCs; (b) Nodal discretization

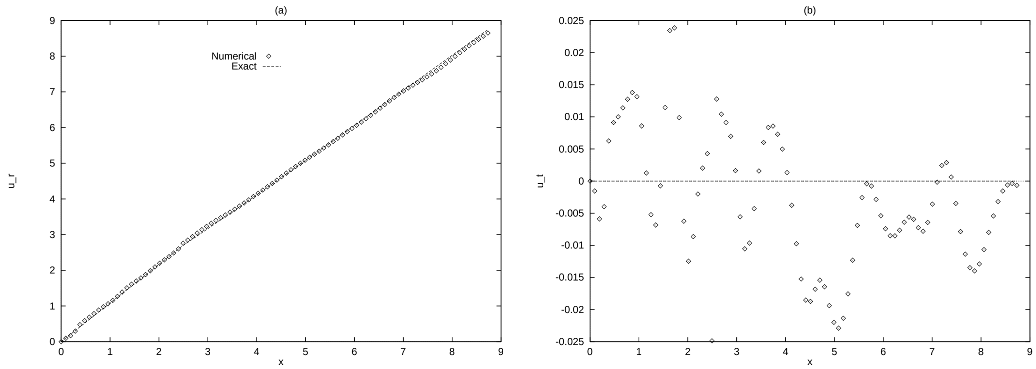

Figure 9: Radial and tangential displacements. (a) u_r; (b) u_θ

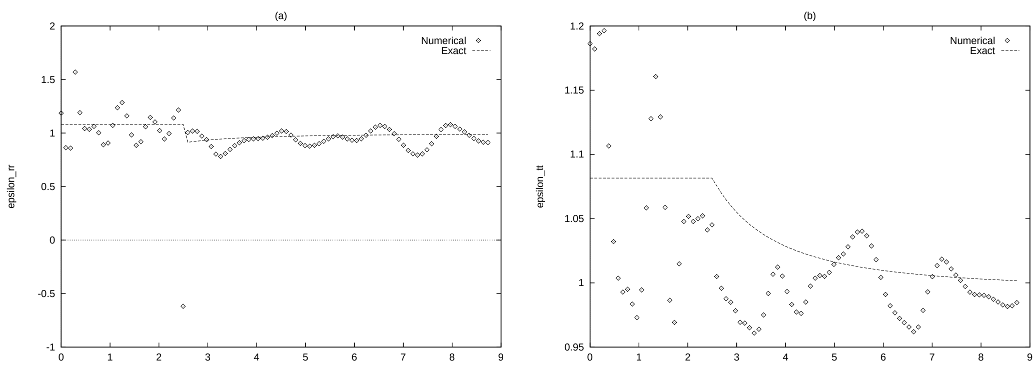

Figure 10: Radial and hoop strains. (a) ε_{rr}; (b) $\varepsilon_{\theta\theta}$

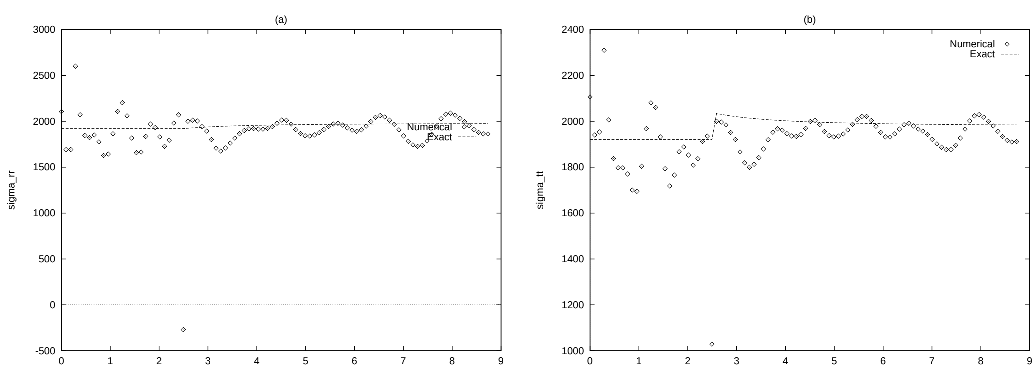

Figure 11: Radial and hoop stresses. (a) σ_{rr}; (b) $\sigma_{\theta\theta}$